

Faithful Simulation and Detection of Quantum Spin Hall Effect on Superconducting Circuits

Jia Liu,¹ Jun-Yi Cao,¹ Gang Chen,^{2,3,*} and Zheng-Yuan Xue^{1,†}

¹*Guangdong Provincial Key Laboratory of Quantum Engineering and Quantum Materials, GPETR Center for Quantum Precision Measurement, and School of Physics and Telecommunication Engineering, South China Normal University, Guangzhou 510006, China*

²*State Key Laboratory of Quantum Optics and Quantum Optics Devices,*

Institute of Laser Spectroscopy, Shanxi University, Taiyuan, Shanxi 030006, China

³*Collaborative Innovation Center of Extreme Optics, Shanxi University, Taiyuan 030006, China*
(Dated: December 21, 2024)

Topological states of quantum matter have inspired both fascinating physics findings and exciting opportunities for applications. Due to the over-complicated structure of, as well as interactions between, real materials, a faithful quantum simulation of topological matter is very important in deepening our understanding of these states. This requirement puts the quantum superconducting circuits system as a good option for mimicking topological materials, owing to their flexible tunability and fine controllability. As a typical example herein, we realize a \mathbb{Z}_2 -type topological insulator featuring the quantum spin Hall effect state, using a coupled system of transmission-line resonators and transmons. The single-excitation eigenstates of each unit cell are used as a pseudo-spin 1/2 system. Time reversal symmetry of the system is proved, and the boundary of the topological phase transition is fixed in the phase diagram. Topological edge states are shown, which can be experimentally verified by detecting the population at the boundary of the plane. Compared to the previous simulations, this compositional system is fairly controllable, stable and less limited. Therefore, our scheme provides a reliable platform for faithful quantum simulations of topological matter.

The discovery of topological matters is a triumph of solid state physics, and since the fractional quantum hall effect was disclosed in 1980s, many theoretical and experimental efforts have been made regarding topological matters. In particular, a new type insulator has been predicted, which has edge current along the surface, but be insulated in the bulk, i.e., the so called quantum spin Hall effect (QSHE) [1–5]. Different from the quantum Hall effect, QSHE has time reversal symmetry and no external magnetic field is needed for its realization. In 2007, the QSHE was discovered in 2D topological insulator HgTe/CdTe system [6]. From then on, many experiments were carried out for the realization of various types of topological matters [7–10]. Although many topological materials had been predicted theoretically, the realization is very little because that such natural materials are still very lacking. Meanwhile, the complicated structure and fixed interactions in real materials prevent us from analytical investigating the physical origin. Therefore, simulating topological properties in well controllable physical systems still has great significance for exploring more deep-seated topological phenomena and enhancing our understanding of the role of topology in quantum materials.

In the past two decades, many quantum simulation schemes for topological matters have been suggested in the ultracold atoms [11–19] and optical system [20–24]. But it is not easy to simulate topological matters in both atomic and optical systems. In atomic system, it is difficult to implement individual control and the same reason makes the detection of the topological phenomena to be hard neither. For optical system, there is always limitations of the interactions, e.g., the hopping phase could not be controlled freely in experiment [14]. In addition, in optical systems, most proposals concern with spinless bosonic system and not suitable for simulating spinful systems.

Recently, superconducting circuits [25–28], a scalable quantum computation platform, has been applied to simulate quantum many-body systems [29–38]. In the spin concern system [39–41], the hopping between each quasi-lattice could be adjusted separately and there is no limitation on nearly all parameters that are used to fix the physical properties of the system, such as the hopping strength, on site potential, hopping phase, etc. Here, we propose a coupled transmission-line resonators (TLRs) and transmons system to simulate a 2D topological insulator. We vary the coupling coefficients and hopping phases of the system, fix the parameters where the system is the topological insulator. Phase diagram is fixed to show where the QSHE can be realized. We also give out the edge states' distribution for special cases, which can be detected by resonance absorption experimentally.

As shown in Fig. 1(a), we consider a 2D lattice with the following model Hamiltonian [14]

$$\mathcal{H} = -t_0 \sum_{m,n} \mathbf{c}_{m+1,n}^\dagger e^{i\hat{\theta}_x} \mathbf{c}_{m,n} + \mathbf{c}_{m,n+1}^\dagger e^{i\hat{\theta}_y} \mathbf{c}_{m,n} + \text{H.c.} + \sum_{m,n} \lambda_{m,n} \mathbf{c}_{m,n}^\dagger \mathbf{c}_{m,n}, \quad (1)$$

where t_0 is the nearest-neighbor hopping strength; $\mathbf{c}_{m,n} = (c_{m,n,\uparrow}, c_{m,n,\downarrow})^T$ is a 2-component operator defined on a lattice site ($x = ma, y = nb$) with a and b being the lattice spacings and m and n being integers; $\hat{\theta}_x = 2\pi\alpha y\sigma_z$ and $\hat{\theta}_y = 2\pi\beta\sigma_x$ with (σ_x, σ_z) being the Pauli matrices and (α, β) being parameters governed by the magnetic flux and spin mixing; $\lambda_{m,n}$ is the on site potential which is here set to be staggered in y -direction, i.e., $\lambda_{m,n} = (-1)^n \lambda$. Define the time reversal operator as $\mathcal{T} = i\sigma_y K$, where σ_y is also the Pauli matrix and K denotes the complex conjugation. We can verify the Hamiltonian in Eq. (1) has the time reversal symmetry, so

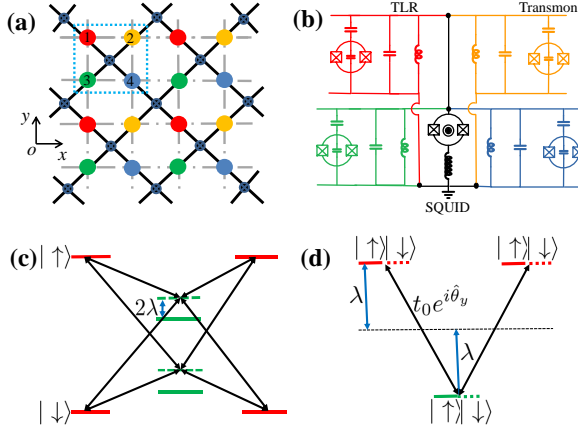


FIG. 1. The proposed setup for QSHE simulation. (a) The proposed 2D JC lattice with each unit contains four sites, illustrated by different colors, with one SQUID connected them, as detailed in (b). (b) Each site consists of one transmon coupled to a TLR, the hopping between neighboring sites is realized by the SQUID. Different Peierls phases of the hoppings in x and y directions can be realized by setting appropriate parameters in the corresponding lattice and the SQUID. (c) Taking out one column in (a) for explanation. For the hopping between the lattices in y -direction 1-3-1, set the detuning in the No. 3 of each two lattices in y -direction, after unitary transformation we can get the staggered on-site potential as shown in (d). (d) Interacted lattices with staggered on site potential along y -direction.

this system belongs to topological class with topological index \mathbb{Z}_2 [42] and can be used to realize the QSHE.

Here we first take one rectangle block including four sites to introduce how to achieve the Hamiltonian in Eq. (1). As shown in Fig. 1(a), each circle presents a Jaynes-Cummings (JC) model made of one TLR and transmon, and the lattices are connected by a superconducting quantum interference device (SQUID) and an inductor L [28]. The hoppings between nearest-neighbor lattices with Peierls phases $\theta_{x,y}$ can be adjusted by tuning the magnetic field through the connected SQUID. The hoppings in x -direction and y -direction are independent from each other and could be realized in the similar way. The Hamiltonian of that JC lattice is

$$\mathcal{H}_{\text{JC}} = \sum_{\mathbf{r}} h_{\mathbf{r}} + \sum_{\langle \mathbf{r}\mathbf{r}' \rangle} J_{\mathbf{r}\mathbf{r}'}(t) (\hat{a}_{\mathbf{r}}^{\dagger} \hat{a}_{\mathbf{r}'} + \text{H.c.}), \quad (2)$$

where \mathbf{r} is the label of the unit cell at (x, y) ; $h_{\mathbf{r}} = \hbar\omega_{\mathbf{r}}(\sigma_{\mathbf{r}}^{+}\sigma_{\mathbf{r}}^{-} + \hat{a}_{\mathbf{r}}^{\dagger}\hat{a}_{\mathbf{r}}) + g_{\mathbf{r}}(\sigma_{\mathbf{r}}^{+}\hat{a}_{\mathbf{r}} + \sigma_{\mathbf{r}}^{-}\hat{a}_{\mathbf{r}}^{\dagger})$ is the JC Hamiltonian in unit cell at \mathbf{r} ; $\sigma_{\mathbf{r}}^{+} = |e\rangle_{\mathbf{r}}\langle g|$ and $\sigma_{\mathbf{r}}^{-} = |g\rangle_{\mathbf{r}}\langle e|$ are the raising and lowering operators of the transmon qubit at \mathbf{r} ; $\hat{a}_{\mathbf{r}}$ and $\hat{a}_{\mathbf{r}}^{\dagger}$ are the annihilation and creation operators of the photon in the TLR at \mathbf{r} ; $J_{\mathbf{r}\mathbf{r}'}(t)$ is the inter-cell hopping strength between the unit cell in \mathbf{r} and its neighbor cells. In the following of the paper, for each $\mathbf{r}' = (ma, nb)$ we set $\mathbf{r} = (ma, (n+1)b)$ or $\mathbf{r} = ((m+1)a, nb)$. The lowest three eigenstates of the JC Hamiltonian $h_{\mathbf{r}}$ are denoted as $|0g\rangle_{\mathbf{r}}$, $|\uparrow\rangle_{\mathbf{r}} = (|0e\rangle_{\mathbf{r}} + |1g\rangle_{\mathbf{r}})/\sqrt{2}$ and $|\downarrow\rangle_{\mathbf{r}} = (|0e\rangle_{\mathbf{r}} - |1g\rangle_{\mathbf{r}})/\sqrt{2}$, where $|ng\rangle_{\mathbf{r}}$ and $|ne\rangle_{\mathbf{r}}$ ($n = 0, 1, 2, \dots$) are the states containing n photons while the transmon is at the ground and ex-

cited states. The corresponding eigen-energies are $E_{\mathbf{r},0g} = 0$ and $E_{\mathbf{r},\uparrow/\downarrow} = \omega_{\mathbf{r}} \pm g_{\mathbf{r}}$. We choose the two single-excitation eigenstates $|\uparrow\rangle_{\mathbf{r}}$ and $|\downarrow\rangle_{\mathbf{r}}$ to simulate the effective spin-up and spin-down states in the lattice at \mathbf{r} . We can control each hopping separately by adjusting the pulse shape of $J_{\mathbf{r}\mathbf{r}'}(t)$. Based on the current experiments [26], setting $t_0/2\pi = 3$ MHz, $\omega_1/t_0 = 2700$, $\omega_2/t_0 = 3000$, $\omega_3/t_0 = 2650$, and $\omega_4/t_0 = 2900$. And $g_1/t_0 = 250$, $g_2/t_0 = 150$, $g_3/t_0 = 150$, $g_4/t_0 = 200$. With those, the energy interval $|E_{\mathbf{r},\eta} - E_{\mathbf{r}',\eta'}|$ of the 16 hopping between each two of them is much larger than (or equal to) 20 times of the effective hopping strength t_0 , such distance is enough for selective frequency addressing. And the hopping strength $J_{\mathbf{r}\mathbf{r}'}(t)$ contains 16 tunes,

$$J_{\mathbf{r}\mathbf{r}'}(t) = \sum_{\eta,\eta'} 4t_{0,\mathbf{r}\mathbf{r}'\eta\eta'} \cos(\omega_{\mathbf{r}\mathbf{r}'\eta\eta'}t + s_{\mathbf{r}\mathbf{r}'\eta\eta'}\varphi_{\mathbf{r}\mathbf{r}'\eta\eta'}), \quad (3)$$

where $s_{\mathbf{r}\mathbf{r}'\eta\eta'} = \text{sgn}(E_{\mathbf{r},\eta} - E_{\mathbf{r}',\eta'})$ is the sign of the hopping phase, and $\omega_{\mathbf{r}\mathbf{r}'\eta\eta'} = |E_{\mathbf{r},\eta} - E_{\mathbf{r}',\eta'}|$ is the energy difference between the nearest lattice. $4t_{0,\mathbf{r}\mathbf{r}'\eta\eta'}$ and $s_{\mathbf{r}\mathbf{r}'\eta\eta'}\varphi_{\mathbf{r}\mathbf{r}'\eta\eta'}$ are the amplitudes and phases corresponding to the hopping $|\eta\rangle_{\mathbf{r}} \rightarrow |\eta'\rangle_{\mathbf{r}'}$, respectively. In experiments, this time-dependent coupling strength $J_{\mathbf{r}\mathbf{r}'}(t)$ can be realized by adding external magnetic fluxes with dc and ac components through the SQUIDs [41]. Both the hopping strengths and phases can be controlled by inducing controllable spin transition process in a certain rotating frame via Eq. (3).

We proceed to show directly how the selective control of individual hopping in the JC lattice can be achieved by adjusting $J_{\mathbf{r}\mathbf{r}'}(t)$ in Eq. (3) via the ac flux. First mapping the Hamiltonian in Eq. (2) into the single excitation subspace by using $|\eta\rangle_{\mathbf{r}}$ to denote one excitation state with 'spin' $\eta = \uparrow, \downarrow$ and get the Hamiltonian in the dressed states,

$$\mathcal{H}_{\text{JC}}^S = \sum_{\mathbf{r},\eta} E_{\mathbf{r},\eta} |\eta\rangle_{\mathbf{r}} \langle \eta| + \frac{1}{2} \sum_{\mathbf{r}\mathbf{r}',\eta\eta'} J_{\mathbf{r}\mathbf{r}'}(t) |\eta\rangle_{\mathbf{r}} \langle \eta'| + \text{H.c.} \quad (4)$$

Then for each $J_{\mathbf{r}\mathbf{r}'}(t)$, we add four tunes, each in resonant to one of the 16 inter-cell hoppings [41], and contains its independent tunable amplitude, frequency and phase as shown in Eq. (3). The form of $J_{\mathbf{r}\mathbf{r}'}(t)$ will be determined by $t_{0,\mathbf{r}\mathbf{r}'\eta\eta'}$ and $\varphi_{\mathbf{r}\mathbf{r}'\eta\eta'}$ depending on the topological phase in simulated scheme. The target Hamiltonian we need to simulate topological insulator could be got in the rotating frame transformed by $U = \exp\{-i[\sum_{\mathbf{r}} h_{\mathbf{r}} - (-1)^{n_{\mathbf{r}}} \lambda(|\uparrow\rangle_{\mathbf{r}}\langle\uparrow| + |\downarrow\rangle_{\mathbf{r}}\langle\downarrow|)]t\}$, where $n_{\mathbf{r}}$ is the same number as n in the $\mathbf{r} = (x, y) = (ma, nb)$. After the unitary transformation $\mathcal{H}'_{\text{JC}} = U^{\dagger} \mathcal{H}_{\text{JC}} U + i\dot{U}^{\dagger} U$, and if the conditions $\{t_{0,\mathbf{r}\mathbf{r}'\eta\eta'}\}_{\eta,\eta'=\uparrow,\downarrow} \ll \{\omega_{\mathbf{r}\mathbf{r}'\eta\eta'}, \omega_{\mathbf{r}\mathbf{r}'\eta\eta'} - \omega_{\mathbf{r}\mathbf{r}'\bar{\eta}\bar{\eta}'}\}_{\eta,\eta'=\uparrow,\downarrow; \omega_{\mathbf{r}\mathbf{r}'\eta\eta'} \neq \omega_{\mathbf{r}\mathbf{r}'\bar{\eta}\bar{\eta}'}}$ are satisfied, all the other terms are fast rotating term that can be dropped with the rotating wave approximation. As a result, we derive the 2D tight-binding model with tunable hopping

coefficients as

$$\begin{aligned} \mathcal{H}_{\text{TB}} = & \sum_{\langle \mathbf{r}\mathbf{r}' \rangle} \sum_{\eta, \eta'} t_{0, \mathbf{r}\mathbf{r}'\eta\eta'} e^{i\varphi_{\mathbf{r}\mathbf{r}'\eta\eta'}} \hat{c}_{\mathbf{r}, \eta}^\dagger \hat{c}_{\mathbf{r}', \eta'} + \text{H.c.} \\ & + \sum_{\mathbf{r}} (-1)^n \lambda \sigma_{\mathbf{r}}^0, \end{aligned} \quad (5)$$

where $t_{0, \mathbf{r}\mathbf{r}'\eta\eta'}$ is just the effective coupling strength and $\hat{c}_{\mathbf{r}, \eta}^\dagger = |\eta\rangle_{\mathbf{r}} \langle G|$ is the creation operator of quasi-electron with ‘spin’ η in the lattice at \mathbf{r} . Comparing the Hamiltonian in Eqs. (1) and (5), we should choose appropriate $t_{0, \mathbf{r}\mathbf{r}'\eta\eta'}$ and $\varphi_{\mathbf{r}\mathbf{r}'\eta\eta'}$ to get the target model in Eq. (1). In x -direction, choose

$$\begin{aligned} t_{0, ((m+1), n), (m, n), \uparrow\uparrow} &= t_{0, ((m+1), n), (m, n), \downarrow\downarrow} = t_0, \\ \varphi_{((m+1), n), (m, n), \uparrow\uparrow} &= 2n\pi\alpha, \\ \varphi_{((m+1), n), (m, n), \downarrow\downarrow} &= -2n\pi\alpha. \end{aligned} \quad (6)$$

And in y -direction, set

$$\begin{aligned} t_{0, (m, (n+1)), (m, n), \uparrow\uparrow} &= t_{0, (m, (n+1)), (m, n), \uparrow\downarrow} \\ &= t_{0, (m, (n+1)), (m, n), \downarrow\uparrow} = t_{0, (m, (n+1)), (m, n), \downarrow\downarrow} = t_0, \\ \varphi_{0, (m, (n+1)), (m, n), \uparrow\uparrow} &= \varphi_{0, (m, (n+1)), (m, n), \uparrow\downarrow} \\ &= \varphi_{0, (m, (n+1)), (m, n), \downarrow\uparrow} = \varphi_{0, (m, (n+1)), (m, n), \downarrow\downarrow} = 2\pi\beta. \end{aligned} \quad (7)$$

When all other coefficients not mentioned above are set to be zero, we could realize the tight binding model in Eq. (1). Equations (6) and (7) show that t_0 could be adjusted by the corresponding hopping strength and (α, β) could be varied through changing hopping phases.

In experiments, adding detuning to the transition frequencies between the nearest-neighbor lattice in y -direction could also simulate staggered on-site potential. We take the column 1-3-1 to illustrate how the detuning is added as in Figs. 1(c) and 1(d). And the hopping strength could be controlled by varying the amplitudes of each unit cell. The hopping phase could be adjusted by the SQUIDs between each lattices, which could drive phase transition between topological and trivial phases. That Peierls phase is hard to implement in cold atom systems because of the limitation that β can not be small values [14].

The validity of individual frequency addressing of the inter-cell transitions can be verified by numerical simulation. We find that in the present of the unmatched driving, all the initial non-target states remain almost unchanged, thus justify our individual frequency addressing method. So far, we have shown how to realize 2D tight-binding model by the combined TLRs and transmons system, next we will use this system simulate the 2D lattice in Fig. 1(a).

Taking periodic boundary condition in x -direction, we numerically calculate the topological invariant [43–45] and fix phase diagrams with corresponding Fermi energy, using the methods for analysing the \mathbb{Z}_2 topological insulators [1, 46]. In the numerical work we set the hopping coefficient t_0 as energy unit, lattice spacings $a, b = 1$ and $\alpha = 1/3$.

When $\beta = 0$ there is no spin-mixing, and if $\lambda = 0$ the Hamiltonian in Eq. (1) are just two Hofstadter models with

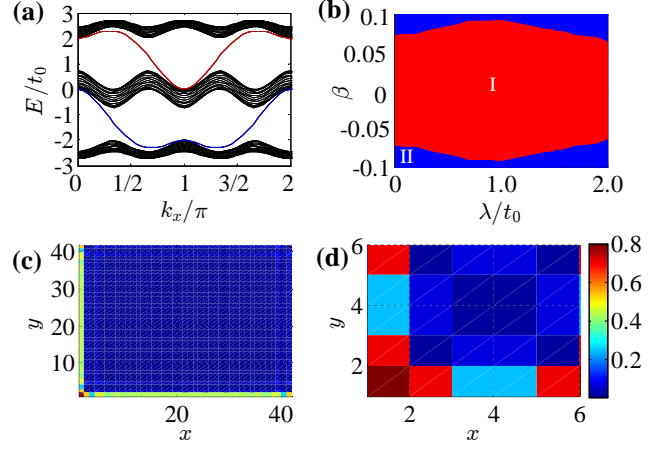


FIG. 2. (a) Energy band for $\lambda = 0$ without spin-mixing $\beta = 0$. (b) Phase diagram in $\beta - \lambda$ plane, based on the band structure in (a) with Fermi energy between t_0 to $2t_0$. The plane is divided into two kinds: (I). topological insulator with edge states which is shown the so called QSHE; (II). metal state. (c), (d) Distributions of the edge states' wave functions for (c) 42×42 and (d) 6×6 lattices.

different magnetic fluxes $\pm 2\alpha\pi$ for spin-up and spin-down branches. With the parameter $\lambda = 0$ and $\beta = 0$ the band structure of the system is plotted in Fig. 2(a). With the numerical results of topological invariants, we can get Fig. 2(b), which is the phase diagram with Fermi energy between t_0 to $2t_0$. The phase is divided into two kinds: topological and metal states. Based on this phase diagram we will show the effective quantum simulation of the QSHE in our system. We did numerical calculation and the wave functions of spin up topological state for different lattice sizes are shown in Figs. 2(c) and 2(d). Considering the symmetry of the system, in this paper we only show the wave function of spin up state. Along $\beta = 0$ axis driving staggered potential λ from 0 to t_0 , there is no phase transition but the QSHE will be affected and the wave distribution will change, such variation could be found in Figs. 2(c,d) and 3(c,e). And the wave function distributions on the surface in Figs. 2(c) and 3(c) show the edge states along the boundary, which is just the perfect simulation of the QSHE. There is size effect in numerical calculation which we will discuss latter and we found a 42×42 lattice is sufficient to cover all details of the physical system.

We next show how to trigger phase transition between topological insulator and metal state by changing the coupling parameter β between spin-up and spin-down terms. In our scheme, adjusting the SQUIDs between lattices along y -direction could varying β in Eq. (1), different from cold atom case [14], there is no limitation of the value of β , it is not necessary to set β to be a large value which means spin-up and spin-down states have to be mixed deeply. Look at Figs. 2(c) and 2(d), when $\lambda = 0$, no spin-mixing case $\beta = 0$, the system is topological insulator and if the spin-mixing efficient became larger the system will transform to metal state at last. We choose $\lambda = t_0$, $\beta = 0$ and 0.1 to show that phase transi-

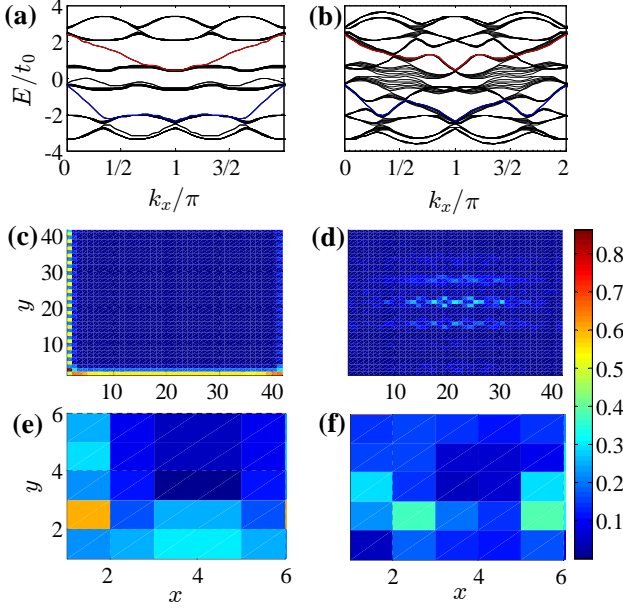


FIG. 3. (a), (b) Band structures for $\lambda = t_0$ with different spin-mixing terms for (a) $\beta = 0$ and (b) $\beta = 0.1$. (c), (e) The wave functions of the topological state with the same parameters as (a). (d), (f) The wave functions of the metal state with the same parameters as (b). (c, d) are the results for 42×42 lattice, while (e, f) are the 6×6 case.

tion. Figures 3(a) and 3(b) are the band structures for $\lambda = t_0$, and different spin-mixing terms $\beta = 0$ and $\beta = 0.1$. And in the same column are the wave functions of the corresponding spin up state for systems of 42×42 and 6×6 lattices. In Figs. 3(c) and 3(e), topological invariant $\nu = 1$ and edge states appear along the boundary of the system. While Figs. 3(d) and 3(f) show the wave functions for the metal states.

Comparing (c), (e) and (d), (f) in Fig. 3, predictably we see the size effects in these new results in Figs. 3(e) and 3(f). However, when $\lambda = 0$ and $\beta = 0$, see Figs. 2(c) and 2(d), the QSHE is not changed so much as $\lambda = t_0$ and $\beta = 0$ case. After numerical calculation, we find $m, n \geq 6$ is good enough to realize the QSHE, and of course the more the better. And mark $\alpha = 1/q$, where q is an integer, set n be an integral multiple of q could effectively reduce the size effects. Considering the real status of experiments $n = 6$ could be a good choice for the present $\alpha = 1/3$.

With the parameters of the edge states shown in Figs. 2(c) and 2(d), prepare an original spin up state $|\uparrow\rangle_r$ with energy around E_{topo} of the edge states. Theoretically, only the lattices at the boundary of the 2D plane that will have excited states and photons could be detected, that is the so called QSHE. Considering the progress of the experiments about the superconducting circuits, there is limitation of the lattices' size in experiment for realizing the QSHE. As shown in Fig. 2(d), 6×6 lattice is enough to find the edge state, and can be achieved experimentally soon [47–50].

As an addition, we investigate the quantum decoherence effects in our proposal for detecting the edge states. We use the

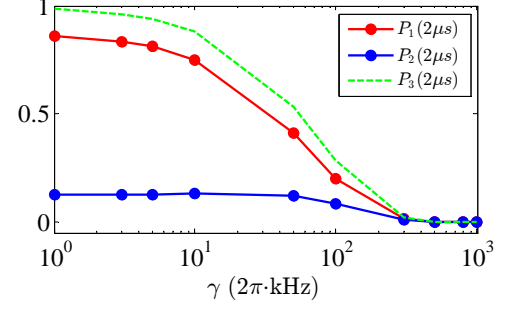


FIG. 4. The edge-site population $P_1(t)$, the inter-site population $P_2(t)$ and the total population of the system $P_3 = P_1 + P_2$ versus the decay rate γ for 6×6 lattice in Fig. 2(d) for the initial state $|\uparrow\rangle_r$ at $r = (1, 1)$. All the results take evolution time $2\mu s$.

Lindblad master equation and take three main decoherence factors in numerical calculation: the losses of the photon, the decay and dephasing of the transmon into account. The Lindblad master equation can be written as

$$\dot{\rho} = -i[\mathcal{H}_{JC}, \rho] + \sum_{\mathbf{r}} \sum_{i=1}^3 \gamma \left(\Gamma_{\mathbf{r},i} \rho \Gamma_{\mathbf{r},i}^\dagger - \frac{1}{2} \{ \Gamma_{\mathbf{r},i}^\dagger \Gamma_{\mathbf{r},i}, \rho \} \right), \quad (8)$$

where ρ is the density operator of the system, γ is the decay rate or noise strength which are set to be the same here, $\Gamma_{\mathbf{r},1} = a_{\mathbf{r}}$, $\Gamma_{\mathbf{r},2} = \sigma_{\mathbf{r}}^-$ and $\Gamma_{\mathbf{r},3} = \sigma_{\mathbf{r}}^z$ are the photon-loss, transmon-loss and the transmon-dephasing operators in the lattice at \mathbf{r} , respectively. In Fig. 4, we plot the edge-site and the inner-site populations:

$$P_1(t) = \text{tr}[\rho(t) \sum_{\mathbf{r}_{\text{edge}}} (a_{\mathbf{r}}^\dagger a_{\mathbf{r}} + \sigma_{\mathbf{r}}^+ \sigma_{\mathbf{r}}^-)], \quad (9)$$

$$P_2(t) = \text{tr}[\rho(t) \sum_{\mathbf{r}_{\text{inner}}} (a_{\mathbf{r}}^\dagger a_{\mathbf{r}} + \sigma_{\mathbf{r}}^+ \sigma_{\mathbf{r}}^-)],$$

after $2\mu s$ for different decay rates. It shows that both the edge state population P_1 and the inner state population P_2 decrease smoothly when the decay rate increases. Fortunately, the detection in our scheme can tolerate the decay rate up to the order of $2\pi \times 10$ kHz, while the typical decay rate is $2\pi \times 5$ kHz. We use initial state $|\uparrow\rangle_{r=(1,1)}$ in the numerical calculation in the consideration that it is easier to preparing such excited state in one site than the eigenstate of the Hamiltonian in Eq. (1) which concerns all 36 sites on the 2D plane. That initial state caused a little leakage from edge state to inner state, however that not effects much in the detection.

In summary, we have proposed a circuit quantum electrodynamics system with TLRs and transmons connected by SQUIDs, the hopping coefficients between these quasi-lattices could be adjusted separately. With that a \mathbb{Z}_2 topological insulator in 2D lattices is realized and the phase transitions between topological and trivial states are simulated. With different parameters the wave functions for metal and topological states are shown all over the 2D lattices separately and

edge states of topological states along the boundaries are illustrated. Considering the real status of superconducting circuits experiment, based on an 6×6 lattice, we have given out a probable proposal to detect the topological edge state which could tolerate the decoherence at present experiments. Our proposal is stable and well controllable, especially using SQUIDs to realize the hopping is smooth and steady. The state of each quasi-lattice could be prepared and detected separately and precisely. These new characteristics surpass the previous methods and will shed light not only on the realization of the topological systems but also topological quantum computation.

We would like to thank F.-L. Gu and D.-W. Zhang for helpful discussions. This work was supported by the National Natural Science Foundation of China (Grant No. 11874156, No. 11904111, and No. 11674200), the Key R&D Program of Guangdong province (Grant No. 2018B030326001), the National Key R&D Program of China (Grant No. 2016YFA0301803) and the Project funded by China Postdoctoral Science Foundation (Grant No. 2019M652684).

* chengang971@163.com

† zyxue83@163.com

- [1] C. L. Kane and E. J. Mele, *Phys. Rev. Lett.* **95**, 146802 (2005).
- [2] C. L. Kane and E. J. Mele, *Phys. Rev. Lett.* **95**, 226801 (2005).
- [3] B. A. Bernevig, T. L. Hughes, and S.-C. Zhang, *Science* **314**, 1757 (2006).
- [4] B. A. Bernevig and S.-C. Zhang, *Phys. Rev. Lett.* **96**, 106802 (2006).
- [5] X.-L. Qi and S.-C. Zhang, *Phys. Today* **63** (1), 33 (2010).
- [6] M. König, S. Wiedmann, C. Brüne, A. Roth, H. Buhmann, L. W. Molenkamp, X.-L. Qi, and S.-C. Zhang, *Science* **318**, 766 (2007).
- [7] M. Z. Hasan and C. L. Kane, *Rev. Mod. Phys.* **82**, 3045 (2010).
- [8] X.-L. Qi and S.-C. Zhang, *Rev. Mod. Phys.* **83**, 1057 (2011).
- [9] A. Bansil, H. Lin, and T. Das, *Rev. Mod. Phys.* **88**, 021004 (2016).
- [10] F. Duncan M. Haldane *Rev. Mod. Phys.* **89**, 040502 (2017).
- [11] D. Jaksch and P. Zoller, *New J. Phys.* **5**, 56 (2003).
- [12] S.-L. Zhu, H. Fu, C.-J. Wu, S.-C. Zhang, and L.-M. Duan, *Phys. Rev. Lett.* **97**, 240401 (2007).
- [13] G.-C. Liu, S.-L. Zhu, S.-J. Jiang, F.-D. Sun, and W.-M. Liu, *Phys. Rev. A* **82**, 053605 (2010).
- [14] N. Goldman, I. Satija, P. Nikolic, A. Bermudez, M. A. Martin-Delgado, M. Lewenstein, and I. B. Spielman, *Phys. Rev. Lett.* **105**, 255302 (2010).
- [15] F. Mei, S.-L. Zhu, X.-L. Feng, Z.-M. Zhang, and C.-H. Oh, *Phys. Rev. A* **84**, 023622 (2011).
- [16] N. Goldman, J. C. Budich, and P. Zoller, *Nat. Phys.* **12**, 639 (2016).
- [17] C. Gross and I. Bloch, *Science* **357**, 995 (2017).
- [18] D.-W. Zhang, Y.-Q. Zhu, Y.-X. Zhao, H. Yan, and S.-L. Zhu, *Adv. Phys.* **67**, 253 (2018).
- [19] N. R. Cooper, J. Dalibard, and I. B. Spielman, *Rev. Mod. Phys.* **91**, 015005 (2019).
- [20] L. Lu, J. D. Joannopoulos, and M. Soljačić, *Nat. Photonics* **8**, 821 (2014).
- [21] V. Peano, C. Brendel, M. Schmidt, and F. Marquardt, *Phys. Rev. X* **5**, 031011 (2015).
- [22] S. D. Huber, *Nat. Phys.* **12**, 621 (2016).
- [23] Y.-P. Wag, W.-L. Yang, Y. Hu, Z.-Y. Xue, and Y. Wu, *npj Quantum Inf.* **2**, 16015 (2016).
- [24] T. Ozawa, H. M. Price, A. Amo, N. Goldman, M. Hafezi, L. Lu, M. C. Rechtsman, D. Schuster, J. Simon, O. Zilberberg, and I. Carusotto, *Rev. Mod. Phys.* **91**, 015006 (2019).
- [25] J. Q. You and F. Nori, *Nature (London)* **474**, 589 (2011).
- [26] M. H. Deveret and R. J. Schoelkopf, *Science* **339**, 1169 (2013).
- [27] Z.-L. Xiang, S. Ashhab, J. Q. You, and F. Nori, *Rev. Mod. Phys.* **85**, 623 (2013).
- [28] X. Gu, A.F. Kockum, A. Miranowicz, Y.-X. Liu, and F. Nori, *Phys. Rep.* **718-719**, 1 (2017).
- [29] A. A. Houck, H. E. Tureci, and J. Koch, *Nat. Phys.* **8**, 292 (2012).
- [30] Y. Salathé, M. Mondal, M. Oppliger, J. Heinsoo, P. Kurpiers, A. Potočnik, A. Mezzacapo, U. Las Heras, L. Lamata, E. Solano, S. Filipp, and A. Wallraff, *Phys. Rev. X* **5**, 021027 (2015).
- [31] R. Barends, L. Lamata, J. Kelly, L. García-Álvarez, A. G. Fowler, A. Megrant, E. Jeffrey, T. C. White, D. Sank, J. Y. Mutus, *et al.*, *Nat. Commun.* **6**, 7654 (2015).
- [32] P. Roushan, C. Neill, J. Tangpanitanon, V. M. Bastidas, A. Megrant, R. Barends, Y. Chen, Z. Chen, B. Chiaro, A. Dunsworth, *et al.*, *Science* **358**, 1175 (2017).
- [33] E. Flurin, V. V. Ramasesh, S. Hacohe-Gourgy, L. S. Martin, N. Y. Yao, and I. Siddiqi, *Phys. Rev. X* **7**, 031023 (2017).
- [34] K. Xu, J. J. Chen, Y. Zeng, Y. R. Zhang, C. Song, W. X. Liu, Q. J. Guo, P. F. Zhang, D. Xu, H. Deng, K. Q. Huang, H. Wang, X. B. Zhu, D. N. Zheng, and H. Fan, *Phys. Rev. Lett.* **120**, 050507 (2018).
- [35] X.-Y. Guo, C. Yang, Y. Zeng, Y. Peng, H.-K. Li, H. Deng, Y.-R. Jin, S. Chen, D. Zheng, and H. Fan, *Phys. Rev. Appl.* **11**, 044080 (2019).
- [36] Z. Yan, Y. R. Zhang, M. Gong, Y. Wu, Y. Zheng, S. Li, C. Wang, F. Liang, J. Lin, Y. Xu, *et al.*, *Science* **364**, 753 (2019).
- [37] Y. Ye, Z.-Y. Ge, Y. Wu, S. Wang, M. Gong, Y.-R. Zhang, Q. Zhu, R. Yang, S. Li, F. Liang, *et al.*, *Phys. Rev. Lett.* **123**, 050502 (2019).
- [38] W. Cai, J. Han, F. Mei, Y. Xu, Y. Ma, X. Li, H. Wang, Y.-P. Song, Z.-Y. Xue, Z.-Q. Yin, S. Jia, and L. Sun, *Phys. Rev. Lett.* **123**, 080501 (2019).
- [39] Y. Wang, J. Zhang, C. Wu, J.-Q. You, and G. Romero, *Phys. Rev. A* **94**, 012328 (2016).
- [40] Z.-Y. Xue, F.-L. Gu, Z.-P. Hong, Z.-H. Yang, D.-W. Zhang, Y. Hu, and J.-Q. You, *Phys. Rev. Appl.* **7**, 054022 (2017).
- [41] F.-L. Gu, J. Liu, F. Mei, S. Jia, D.-W. Zhang, and Z.-Y. Xue, *npj Quantum Inf.* **5**, 39 (2019).
- [42] A. P. Schnyder, S. Ryu, A. Furusaki, and A. W. W. Ludwig, *Phys. Rev. B* **78**, 195125 (2008).
- [43] T. Fukui, Y. Hatsugai, and H. Suzuki, *J. Phys. Soc. Jpn.* **74**, 1674 (2005).
- [44] M. Kohmoto, *Ann. Phys. (N. Y.)* **160**, 343 (1985).
- [45] Y. Hatsugai, *J. Phys.: Condens. Matter* **9**, 2507 (1997).
- [46] R. Yu, X.-L. Qi, A. Bernevig, Z. Fang, and X. Dai, *Phys. Rev. B* **84**, 075119 (2011).
- [47] A. O. Niskanen, K. Harrabi, F. Yoshihara, Y. Nakamura, S. Lloyd, and J. S. Tsai, *Science* **316**, 723 (2007).
- [48] R. Barends, J. Kelly, A. Megrant, A. Veitia, D. Sank, E. Jeffrey, T. C. White, J. Mutus, A. G. Fowler, B. Campbell, *et al.*, *Nature (London)* **508**, 500 (2014).
- [49] Y. Lu, S. Chakram, N. Leung, N. Earnest, R. K. Naik, Z.-W. Huang, P. Groszkowski, E. Kapit, J. Koch, and D. I. Schuster,

Phys. Rev. Lett. **119**, 150502 (2017).

- [50] C. Neill, P. Roushan, K. Kechedzhi, S. Boixo, S. V. Isakov, V. Smelyanskiy, A. Megrant, B. Chiaro, A. Dunsworth, K. Arya, *et al.*, Science **360**, 195 (2018).